Morphological and Thermal−Mechanical Stretching Properties on Polymeric Lateral Flow Nitrocellulose Membrane

4 AUTHORS:

Abdul Latif Ahmad
Universiti Sains Malaysia
321 PUBLICATIONS **7,830** CITATIONS

SEE PROFILE

Siew Chun Low
Universiti Sains Malaysia
31 PUBLICATIONS **217** CITATIONS

SEE PROFILE

Syamsul Rizal Abd Shukor
Universiti Sains Malaysia
56 PUBLICATIONS **365** CITATIONS

SEE PROFILE

Asma Ismail
Universiti Sains Malaysia
63 PUBLICATIONS **481** CITATIONS

SEE PROFILE

Morphological and Thermal-Mechanical Stretching Properties on Polymeric Lateral Flow Nitrocellulose Membrane

A. L. Ahmad,*,[†] S. C. Low,[†] S. R. Abd. Shukor,[†] and A. Ismail[‡]

School of Chemical Engineering, Engineering Campus, Universiti Sains Malaysia, Seri Ampangan, 14300 Nibong Tebal, S.P.S, Penang, Malaysia, and Institute for Research in Molecular Medicine, Health Campus, Universiti Sains Malaysia, 16150 Kubang Kerian, Kelantan, Malaysia

Lateral flow nitrocellulose (NC) membrane is well-known as the transport medium in a diagnostic test strip. The function of the membrane is greatly influenced by its physical morphology and chemical composition. Hence, a thermal-mechanical stretching technique was introduced to modify polymeric membrane morphologies for various performance studies. Membrane samples were stretched at the appropriate settings of stretching elongation, stretching speed, and stretching temperature. Experimental, AFM, and SEM results show that membrane morphologies changed significantly as a result of the stretching effects. The current study has demonstrated that physical thermal-mechanical stretching properties are important in modifying membrane morphologies for specific applications, since these parameters potentially affect the membrane's final performances. These findings provided some insight on the relationship between stretched membranes' morphology and performances. This knowledge is useful in producing both versatile and durable nitrocellulose membranes for lateral flow applications.

1. Introduction

Lateral flow nitrocellulose (NC) membrane is well-known as the transport medium in a diagnostic test strip[1,2] and immobilization of proteins[3] because of its specific binding affinity to amino acids. The function of the membrane is greatly influenced by its physical morphology and chemical composition.[4,5] Different membrane surface properties, structures, and dimensions are needed for varying diagnostic testing.[6] Hence, study on the behavior of surface and internal layers of the membrane is fundamental in developing the lateral flow membrane as one of the processing materials in medicine and healthcare analysis devices. Precise control of membrane surface and internal layer structure could yield accurate and effective immunological analysis.

However, the formation of membrane morphology cannot depend solely on membrane casting formulation because of extreme chemical inertness and the sensitivity of the casting process to the surroundings. The formation mechanism was said to be rather complex because of the highly variable number of rheological factors that need to be taken care of during the casting stage. It is nearly impossible to mull over all the varieties of mixture components and casting processes to control the membrane morphology to meet the specific requirements. Thus, an idea on modification and improvement of membrane morphology through a thermal mechanical stretching technique under heat treatment is introduced.[7]

The thermal mechanical stretching technique is a technique that transforms mechanical strength and heat treatment to membrane to yield the desired morphology.[8–10] The synthesized membrane was uniaxially stretched in parallel to the casting direction under a certain heating temperature. The purpose of stretching is to modify the membrane structure, while the appropriate level of heat treatment is applied on membrane samples to ensure the polymer is ductile enough to be stretched.

Positive correlations between controlling the membrane pore morphology and the stretching operation were shown by Morehouse et al.[11,12] Modification of membrane pore structure by stretching operation corresponded to increase in membrane flux for cross-flow separation. This finding was in close agreement with Kurumada et al.,[7] which also intentionally modified the PTFE membrane pore dimensions using membrane stretching operations to improve the overall membrane performances.

The microstructure and characterization of stretched and unstretched membrane can be studied under attenuated total reflectance Fourier transform infrared (ATR-FTIR) spectroscopy, field emission scanning electron microscopy (FESEM), and atomic force microscopy (AFM). These powerful morphological techniques generate the membrane morphologies by direct or indirect scanning of the membrane surface,[13] where a detailed and accurate representation of membrane topographical changes and membrane surface characteristics such as roughness, porosity, and surface pore size[14,15] can be obtained.

As for membrane performances, liquid wicking rate (liquid migration time in the membrane layer) and membrane protein binding ability are the two major factors that affect the performance of a stretched NC membrane in diagnostic testing. This has contributed to various fields of study, such as the immuno-chromatography test, protein immobilization analysis, and Western blotting. In immunodiagnostic tests, the lateral wicking rate is the time required to perform the diagnostic (to test the membrane rapidity and effectiveness) while membrane protein binding ability is a measure of the sensitivity of the assay.

Previous studies[7,11,12] focused on the enhancement of cross-flow performance of a membrane through the stretching mechanism. The current study elucidates the microporous structure transformations of the lateral flow NC membrane through the mechanical stretching operation. The experimental design is aimed to illustrate the membrane performances and microstructures between stretched and unstretched membranes. In this paper, the main emphasis is on how the membrane microstructure and morphologies are affected by changing the setting of the stretching operation such as stretching elongation,

---

* To whom correspondence should be addressed. E-mail: chlatif@eng.usm.my. Tel: +6-04-5941012. Fax: +6-04-5941013.
† School of Chemical Engineering.
‡ Institute for Research in Molecular Medicine.

stretching rate, and heating temperature. Two major membrane performances of concern in the present study are membrane protein binding ability (to test the membrane's sensitivity) and membrane wicking ability (to test the membrane lateral migration rapidity).

2. Experimental Methods

2.1. Membrane Preparation. Prior to the stretching operation, the flat sheet NC membrane that was not supported by any backing material was prepared using the dry phase inversion method.[16,17] For NC membrane preparation, the raw materials included nitrocellulose polymer with 11.8−12.3% nitrate and 30% alcohol, the solvent methyl acetate (MA) and the nonsolvent isopropanol (IP). NC polymer (4 wt %) dissolved in 82 wt % MA and 10 wt % IP were prepared. The 2 wt % glycerol additive and 2 wt % water which served as the pore former were added when the NC polymer dissolved completely in MA and IP solution.[16] The casting process was performed with a membrane autocasting machine, where the casting solutions were cast onto a glass plate with a casting blade.[17] The depth of the casting was 700 μm with a casting speed of 100 rpm. Before use, the membranes were dried in a vacuum oven overnight at 40 °C. Ten sheets of membranes were synthesized using similar casting formulation and conditions. Every membrane was characterized in terms of porosity, pore size, and thickness to ensure the same quality and morphology of the membranes produced.[16,17]

2.2. Stretching Operation. Rectangular samples (100 mm × 30 mm) were cut from the synthesized flat sheet membranes. The membrane strip was gripped by a rigid support beam (40 mm long × 10 mm width) on a stretching platform in a heat insulated chamber. The membranes were heated up to the appropriate stretching temperature in the heat insulated chamber by a convective oven which was integrated with a heat distribution blower for uniform air distribution. The temperature sensor was connected to the heat insulated chamber and temperature controller to carry out an accurate temperature measurement. In the selection of suitable stretching temperature, the membrane was heated in the convection oven until the shrinkage of membrane was observed. Temperature near the shrinkage point of the membrane is set as the highest temperature in our study. In this study, 75 °C was found to be the highest stretching temperature. According to Binke et al.,[18] the melting point of NC was found to be at 476.84 K by using the modulated differential scanning calorimetry (MDSC) method. In this study, all the membranes were stretched at a temperature far lower than this temperature, to avoid any transition of solid polymer in the membrane.[18]

The stretching rate was controlled by an electric stepper motor (Vexta EM569-NA, Japan) with a stepping controller (Vexta UDX 5107N, Japan). In the preliminary study, membrane strips were stretched at a stretching rate ranging from 0.04 mm/s to 0.20 mm/s with a constant stretching temperature (50 °C) and stretching elongation (10%). When the stretching speed was more than 0.1 mm/s, the membrane strips were not able to stretch until 10% of the stretching elongation and broke in half, as a result of the higher force which was concentrated on a certain area of the membrane strip. On the basis of this observation, the highest stretching rate was set at 0.1 mm/s. Each sample was stretched uniaxially parallel to the initial membrane casting direction. All samples were stretched at stretching elongation from 4% to 22% of the total membrane sample's length with stretching rate from 0.04 to 0.1 mm/s and stretching temperature ranging from 25 to 75 °C, as shown in

Table 1. Design Layout of Different Stretching Settings for Membrane Morphology Modification

membrane sample	stretching elongation, % of total membrane sample length	stretching temperature, °C	stretching speed, mm/s
1	8	35	0.04
2	18	35	0.04
3	8	35	0.1
4	18	35	0.1
5	8	65	0.04
6	18	65	0.04
7	8	65	0.1
8	18	65	0.1
9	4	50	0.07
10	13	50	0.07
11	22	50	0.07
12	13	24.8	0.07
13	13	75.2	0.07

Table 1. To harden and strengthen the microstructure of the stretched membrane, the membrane sample was annealed for 15 min. The sample was then held under tension and air-cooled to room temperature.[11] In the preliminary study, stretched NC membranes were observed for two months to confirm the possibility of membrane length recovery after stretching. The results have shown insignificant recovery of membrane length in the stretching direction, which was in-line with the observation performed by Morehouse et al. with a polymeric membrane.[11] A total of 10% of the stretched sample area near the stretching edges was not included in any membrane characterization and performance testing since this region did not represent the membrane morphology and pore structure. The experiment was repeated three times for each experimental run. The average value of the experimental data for each membrane sample was obtained.

2.3. Membrane Characterization. 2.3.1. Attenuated Total Reflectance Fourier Transform Infrared (ATR-FTIR). Bonding characterization of the membrane surface was confirmed by the ATR-FTIR instrument (Perkin-Elmer Series II). The membrane samples were clamped onto the horizontal ATR crystal surface (50 mm × 10 mm × 2 mm) fixed at the incidence angle of 45°, yielding approximately 12 internal reflections at the membrane surface. All membrane samples were measured from 400 cm^{-1} to 650 cm^{-1} wavenumber. Commercial membrane from Millipore (HF 240, Hi-Flow Plus Membrane) was used to compare the existing functional groups with those of the synthesized membrane. This Millipore membrane is commonly used in the immunochromatography tests for detecting infectious disease organisms, analyzing drugs of abuse, and and so forth, which have similar application with the membrane developed in this study.

2.3.2. Field Emission Scanning Electron Microscopy (FESEM). The surface and cross section morphologies of the membranes were observed by FESEM (VPFESEM SUPRA 35VP) at an accelerating voltage of 3 kV and a 1000× magnification. Membrane samples were first coated with a conducting layer to prevent charging up of the membrane surface. The membrane was then fractured under liquid nitrogen and mounted on the sample stud by adhesive tape for the cross-sectional observation. From the images, average major and minor axis lengths of the membrane pores were measured. At least 10 spots per sample were measured to confirm the reproducibility of the experimental data. On the other hand, thickness measurement of the membrane was performed by FESEM at four different points on the membrane sample. The membrane thickness was further confirmed using a micro-
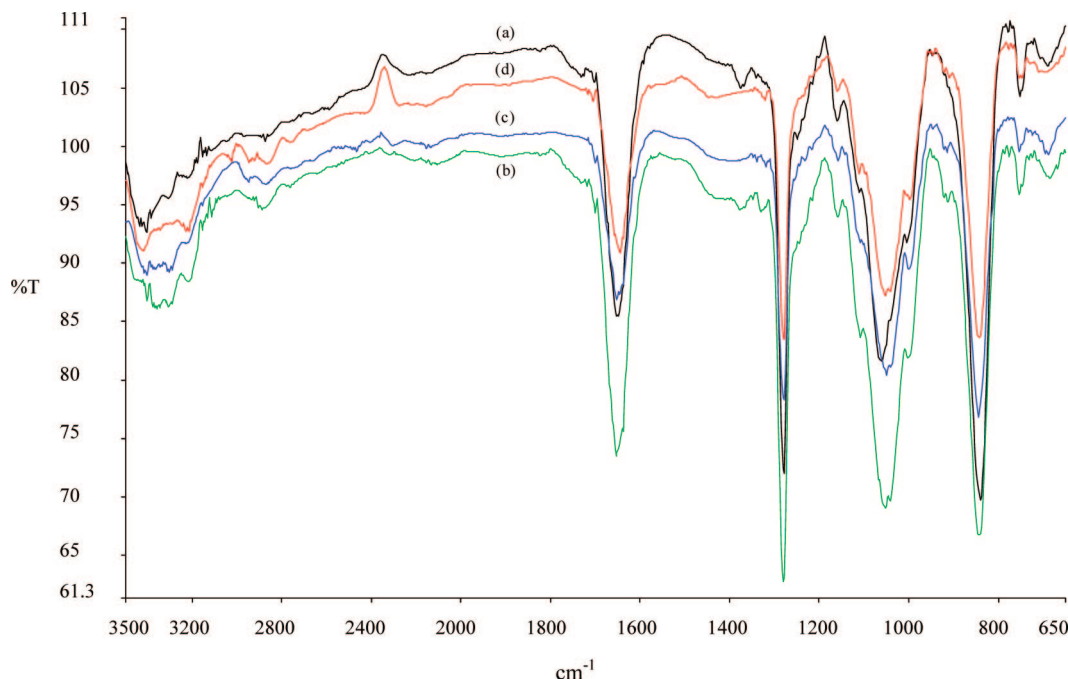
Figure 1. ATR-FTIR spectra of (a) Millipore's membrane, (b) unstretched NC membrane, (c) stretched membrane with 8% stretching elongation, and (d) stretched membrane with 18% of stretching elongation.

thickness gauge (Mitutoyo 7301, Japan), at three different points on the membrane strip.

2.3.3. Atomic Force Microscope (AFM). Surface characterization (roughness and pore structure) of the stretched membrane was performed by AFM (JSTM-4200, JEOL, Japan) equipped with a noncontact head with a spring constant of 45 N m^{-1}. A conical silicon tip cantilever (MikroMash Co.) with full tip cone angle less than 20° was used to scan the specimen surface. Unstretched and stretched membranes were placed on top of a microscope's slide glass with both edges of the membrane taped using double-sided tape to ensure that the samples were totally flattened. The membrane samples were scanned with a laser beam reflected by the cantilever with 30 μm × 30 μm scanning area. All AFM measurements were taken in ambient conditions. The force between the tip and the sample would lead to a deflection of the cantilever based on Hooke's law. The deflection is based on the spot reflection from the top surface of the cantilever into an array of photodiodes. The reflected laser beams were then used to generate a three-dimensional membrane surface topographical image. The image was analyzed with image processing software to identify the membrane surface pore size, roughness, and pore density.[13]

2.3.4. Determination of Membrane Porosity and Pore Size Ratio. According to Yamane et al.[19] and Meier,[20] porosity of the unstretched and stretched membrane can be calculated using the formula

$$\varepsilon = \frac{V_A - V_E}{V_A} \times 100\% \qquad (1)$$

V_A is the apparent volume of the membrane, calculated from the film thickness and the film surface area (2 cm × 1 cm). V_E is the existent volume of the membrane, determined through the corresponding polymer density (1.23 g/cm^3) and membrane sample weight. The porosity of at least three samples of each membrane were measured to confirm the reproducibility of experimental data.

From FESEM, the pore size diameter for elliptical membrane pores was measured. Major and minor axes of the elliptical pores were measured from 10 different locations within the membrane images under FESEM. Average membrane pore size ratio was calculated as the major axis length divided by the minor axis length of the membrane pores.

2.4. Membrane Performances. The stretched membrane performances are the main concern in this study to prove the reproducibility and advantages of the stretching technique. Performance testing such as membrane protein binding ability and wicking rate was carried out according to previous work.[16] The stretched membrane samples were cut into a 2 cm wide and 5 cm long strips for in-plane liquid distribution or liquid's lateral wicking time measurement. Deionized water was used as the wicking medium. The experiment was conducted at room temperature (27 °C) and ambient pressure. Time measurement started when the wicking medium had migrated 4 cm along the membrane strip after initial contact between the membrane and the deionized water (i.e., the wicking medium).

Membrane protein binding ability is commonly accepted as a universal property and reflects the membrane performance in a diagnostic test strip. The stretched membrane binding ability was measured on 12 mm diameter samples, and the total volume of the membrane was calculated. All the membrane samples were incubated in 3 mL of bovine serum albumin (BSA) solution with 0.05 M phosphate buffer (pH 7.0, 3 mg/mL) and shaken for 3 h at 25 °C. Unbound BSA on the membrane surfaces was washed (repeated two times) with phosphate buffer. Each sample replicate was transferred into test tubes. Subsequently, 2 mL of bicinchoninic acid working reagent (Merck, Germany) was added, and the test tubes were incubated at 37 °C for 30 min. The BSA concentration was detected at a 562 nm wavelength using a spectrophotometer (Spectronic Genesys, U.S.A.). Using the preliminarily plotted standard curve, the corrected absorbance readings for the samples were interpolated.

3. Results and Discussion

3.1. ATR-FTIR. Figure 1 shows the analysis of ATR-FTIR spectra. In comparison, (a) commercial membrane, (b) synthesized NC membrane, and (c, d) stretched membranes appeared
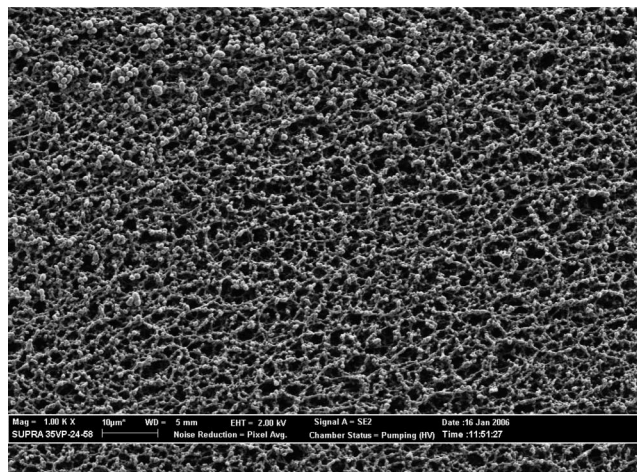
(a)
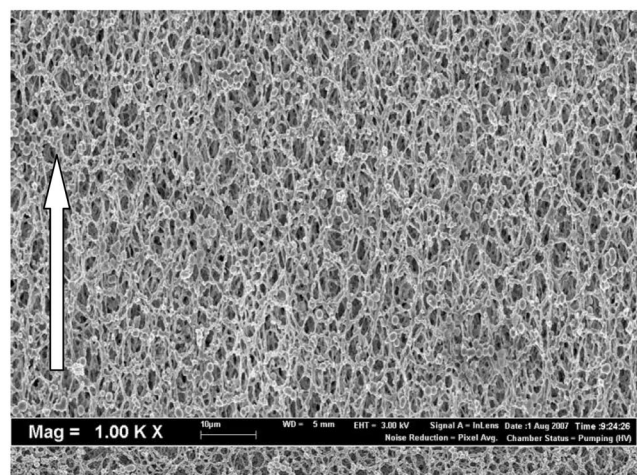
(b)

Figure 2. FESEM micrographs for the surfaces of (a) unstretched membrane and (b) stretched membranes, prepared with stretching elongation of 18% of the total membrane sample.

to have similar ATR spectra bands on the polymer chains. As shown in Figure 1, some peaks such as 1650 cm^{-1} appeared on the synthesized membrane, which corresponded to the symmetric stretching band of $-ONO_2$ groups. This means that the presence of the nitrate group in the synthesized membrane was confirmed. The extremely broad $-OH$ absorption occurring in the region from 3500 cm^{-1} to 3200 cm^{-1} corresponded to the small number of hydroxyl groups in the membrane.[21] Protein molecules that possessed permanent dipoles and polarizable groups on the molecular surface were able to attach to the surface of the membrane by the strong dipole of the nitrate group in the membrane polymer matrix.[21,22] This electrostatic interaction causes an affinity binding between membrane surface and protein molecule that could not be easily forced out or washed from the membrane surface.

3.2. FESEM. Effects of various longitudinal stretching elongations toward the membrane structures were investigated on the morphological observations under FESEM images. Figure 2 showed that both polymer matrixes for (a) unstretched membrane and (b) stretched membrane (22% of stretching elongation) remained as three-dimensional open pores structure.

Subsequently, the FESEM micrograph shows that the membrane's pore arrangement changed with the elongation of the membrane sample. In Figure 2a, the pore size of the unstretched membrane tends to be round and distributed homogeneously in

**Table 2. Characterization of Membrane after Being Stretched**

membrane sample	porosity, %	yield thickness, μm	major pore axis, μm	pore size ratio, (major axis)/ (minor axis)
		Unstretched Membrane		
	72.65 ± 0.21	127 ± 3	4. 50 ± 0.19	
		Stretched Membranes		
1	75.40 ± 0.62	115 ± 3	5.88 ± 0.17	2.56
2	76.19 ± 0.39	108 ± 3	6.59 ± 0.21	2.88
3	74.68 ± 0.83	117 ± 3	5.39 ± 0.24	2.39
4	76.00 ± 0.49	112 ± 2	5.65 ± 0.18	2.51
5	73.99 ± 0.72	111 ± 2	5.08 ± 0.20	2.32
6	74.45 ± 0.50	100 ± 1	5.82 ± 0.29	2.67
7	72.50 ± 0.30	114 ± 4	4.64 ± 0.09	2.12
8	73.83 ± 0.82	107 ± 3	5.28 ± 0.14	2.41
9	73.56 ± 0.59	118 ± 3	4.04 ± 0.08	1.67
10	73.61 ± 0.60	120 ± 4	6.22 ± 0.32	2.59
11	75.74 ± 0.90	104 ± 3	7.16 ± 0.37	3.01
12	76.10 ± 0.31	121 ± 4	7.00 ± 0.38	2.91
13	71.71 ± 0.67	112 ± 3	4.31 ± 0.04	1.82

all directions of the measurement dimension. Meanwhile, for the stretched membrane shown in Figure 2b, the surface pores appeared to be slightly elliptical and highly distributed in the direction in which it was stretched. Since the pores of the stretched membrane appeared to be in an elliptical shape, the major pore axis and minor pore axis in the particular elliptical membrane pores need to be determined. In this study, the proportion of the elliptical pores of the membrane sample, that is, pore size ratio between the major pore axis and the minor pore axis, were increased with increasing membrane elongation, as shown in Table 2. These larger and longer elliptical pore chains thus enhanced the performances of the membrane in lateral flow and binding ability which will be discussed later.

However, it was found that different stretching temperatures and stretching speeds do not significantly modify the membrane pore arrangement within the range of temperatures and rates studied. At a constant stretching elongation, the stretched membranes appeared to have similar membrane surface topography, that is, similar elliptical pore shape arrangement on the membrane surface, as shown in Figure 3. Considering the effect of stretching temperature and stretching rate, the stretched membranes with a same stretching elongation tend to have the same surface pore arrangement in elliptical shapes. The only difference in the membrane structures is the membrane pore size ratio and porosity which will be discussed in section 3.3. A similar observation was also reported by Morehouse et al.[11] who studied the effects of stretching temperature and strain rate on poly(vinylidene fluoride) (PVDF) membrane.

3.3. Pore Ratio, Porosity, and Yield Thickness of Membrane. Table 2 shows the porosity, pore size ratio, and yield thickness of the stretched membrane. The pore size ratio of stretched membrane increased from 1.67 to 3.01 with the increase in the stretching elongation. The same increment was also observed in the membrane's porosity, as shown in Table 2. For example, samples 1 and 2 which had the same stretching temperature and stretching speed resulted in increasing membrane pore size ratio with the increase of membrane major pore axis when they were elongated. With the constant stretching temperature and stretching rate, stretching would introduce higher force on the membrane. Hence, the major pore axis at the stretching direction was increased and the minor pore axis at the perpendicular of the stretching direction was decreased.

In contrast, at the same membrane stretching speed and stretching elongation, the membrane surface porosity and pore size ratio were decreased with quantifiable increase in stretching
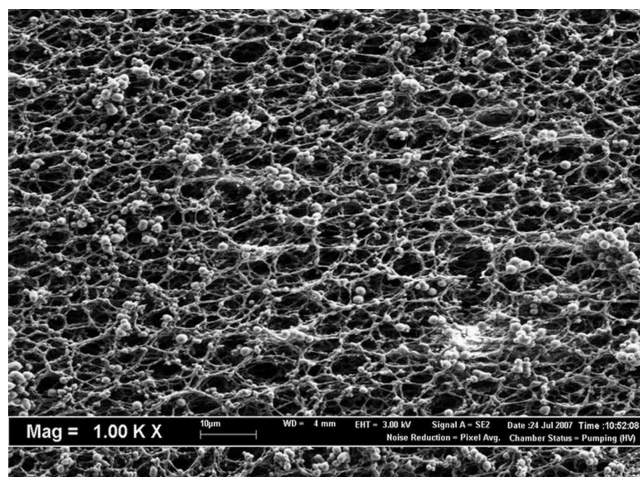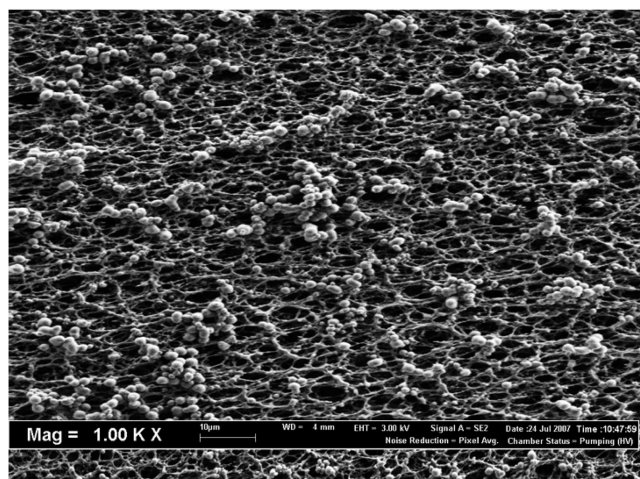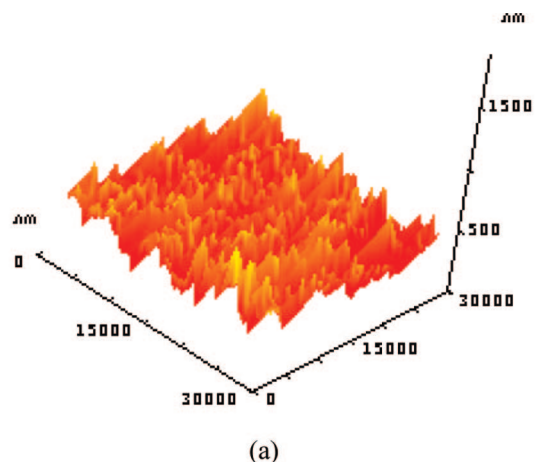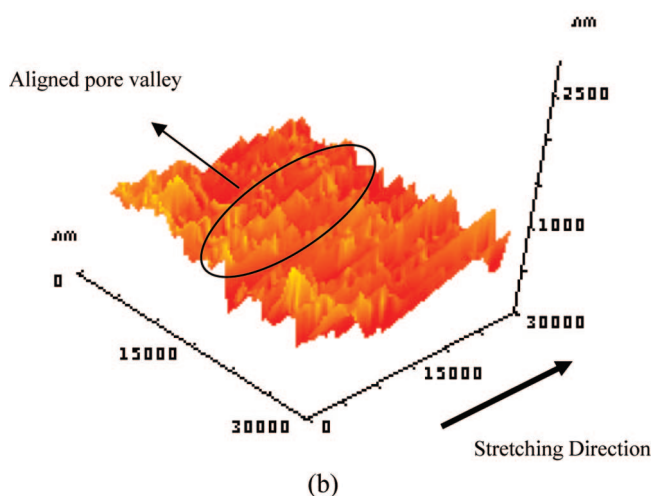
Figure 3. FESEM micrographs for the surfaces of the stretched membrane prepared at (a) 35 °C and (b) 65 °C of the stretching temperature (stretching elongation, 22% of total membrane sample; stretching rate, 0.04 mm/s).

Figure 4. AFM micrographs for the surfaces of (a) unstretched membrane and (b) stretched membrane.

temperature. For example, when the stretching temperatures were increased from 24.8 to 50 °C and 75.2 °C (refer to membrane samples 10, 12, and 13), the membranes' porosity and pore ratio dropped from 76.1% to 71.1% and 2.91 to 1.82, respectively. This is because when higher stretching temperature was introduced, it will cause the agglomeration of polymer matrix in the membrane layers and create closed pores on the membrane surface. These closed pores further reduce the membrane connection voids and finally lower the membrane's porosity, and smaller membrane pore sizes were observed. Similar findings were observed regarding the effects of stretching rate on the membrane morphology. When higher stretching rate was applied during the stretching operation, smaller membrane pore size and lower membrane porosity were observed. This phenomenon is due to the ductility of the polymer. When the membrane was stretched using the higher stretching rate, the stretching force would concentrate on the middle area of the membrane strip. The membrane pores and porosity on this small area will increase dramatically compared to other areas in the membrane strip. In another words, the area of the membrane strip which was not subjected to the stretching force would have an insignificant change in membrane pores and porosity. While measuring the overall membrane mean pore size and porosity, a membrane with smaller pore size and lower

Table 3. RMS Roughness and R_a Roughness for Stretched and Un-Stretched Membrane

membrane	rms (nm)	R_a (nm)
stretched	96.07	150.00
unstretched	74.03	117.39

membrane porosity was observed when the membrane was stretched using a higher stretching rate.

3.4. AFM. To fully characterize the membrane, AFM analysis was performed to study the differences of surface morphologies between stretched and unstretched membranes in addition to FESEM analysis. AFM was used to analyze the morphology, pore size, and roughness of the membrane surfaces. In Figure 4, AFM analysis clearly shows that the membrane structure changed with stretching effects. The unstretched membrane (Figure 4a) has an identical topographical image. The stretched membrane (Figure 4b), in contrast, showed an aligned pore valley along the stretching direction. The aligned pore structure observed from the image topography was in line with the previous findings from FESEM images and membrane characterization from Table 2. This shows that with the stretching effects on the membrane samples, the morphologies and pore structure of the membrane can be modified.[12]

From the AFM analysis, R_a, the mean roughness which stands for the mean value of the surface relative to the center plane, is calculated as[23]

$$R_a = \frac{1}{S} \int_0^a \int_0^b |f(x, y) - z_0| \, dx \, dy \qquad (2)$$

$$z_0 = \frac{1}{S} \int_0^a \int_0^b |f(x, y)| \, dx \, dy \qquad (3)$$

S is the specified area, $f(x, y)$ is the height in the specified area, a and b are the length of the sample, and z_0 is the mean height value. rms roughness, R_{rms}, which represents the deviation of peaks and valleys from the mean plane, is defined as[23]

$$R_{RMS} = \left[\frac{1}{S} \int_0^a \int_0^b \{f(x, y) - z_0\}^2 \, dx \, dy \right]^{1/2} \qquad (4)$$

The R_a and R_{rms} values that were used to correlate surface roughness and effect of stretching are presented in Table 3. Analyzed data suggests that average membrane surface height does not significantly change as a result of the stretching effect. The slight increase of rms and R_a roughness for the stretched membrane (Table 3) could be due to the minor increment of the surface height caused by stretching line (the aligned membranes' pore valleys) on the membrane surface. The changes of membrane surface topography would definitely lead to different lateral membrane performances since the lateral fluid migration trend in the membrane would be different as well due to different pores arrangement in the membrane layers.

3.5. Membrane Performances. Figure 5a shows that longer stretching elongation, 18%, leads to a faster lateral wicking speed. This translated into shorter wicking time for water to migrate to 4 cm height in the membrane layers. The membrane wicking time decreased from 879 s to 681 s and 532 s (refer to membrane samples 9, 10, and 11), for 4%, 13%, and 22% of stretching elongation, respectively. From previous FESEM images and experimental data in Table 2, it was observed that the membrane surface pores and porosity increased when longer stretching elongation was introduced. This indicated that the connection void spaces between the membrane layers were arranged more regularly and tend to reduce the resistance of lateral diffusion along the stretching direction. This regular arrangement on membrane pores would then fasten the lateral wicking rate of the wicking medium.

In contrast, a higher stretching temperature, 65 °C, leads to a slower lateral wicking speed or longer wicking time for water to migrate to 4 cm height in the membrane, as shown in Figure 5b. This is due to the polymer matrix in the multilayer membrane which tended to agglomerate when higher stretching temperature took place. Hence, the polymer matrix bulkiness increased. Increase of membrane polymer rigidity would further decrease the connection voids between the membrane layers and contributed to longer wicking time as shown in Figure 5b. The same trend was observed in Figure 5c, where higher stretching rate led to a slower lateral wicking speed. When the stretching speed increased from 0.02 mm/s to 0.12 mm/s, the lateral wicking time also increased from 525 s to 728 s. This is because when the stretching rate is too high, polymer chains in the membrane layers do not have enough time to distribute the stretching force homogenously and endure higher stretching forces at certain places on the membrane strip. This uneven distribution of stretching force will cause irregular membrane polymer structures and decreases the migration speed of the wicking medium in membrane layers.

Another important factor that affects stretched membrane performance is the membrane protein binding ability. On the basis of Figure 6a, with increasing stretching, the membrane protein-binding ability decreased. This is due to the increment in membrane pore size with quantifiable membrane elongation.
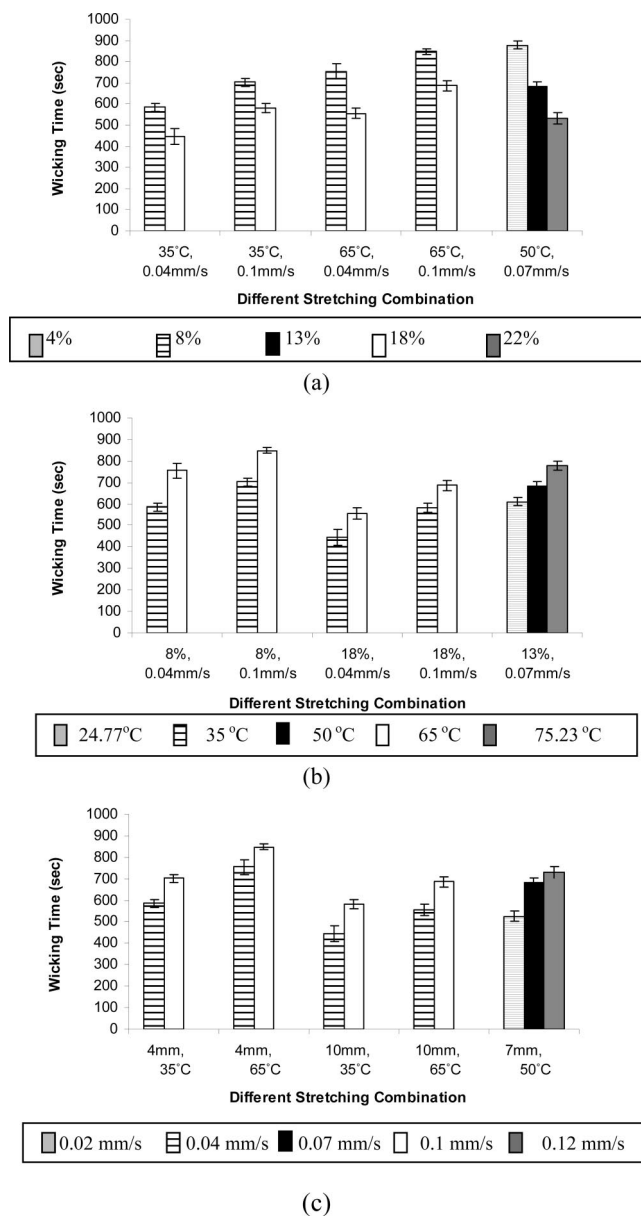
(a)

(b)

(c)

Figure 5. Effects of (a) stretching elongation, (b) stretching temperature, and (c) stretching speed on membrane lateral wicking performance: wicking time needed for testing medium migrated 4 cm up the height of the membrane strip. Each value represents an average value of 3 data and the bars represent the standard error.

Larger pores and porosity of the stretched membrane would decrease the total surface area for electrostatic binding between protein molecules and membrane. A similar trend was observed in Figure 6b.

As the stretching temperature increased from 35 to 65 °C, the membrane protein-binding ability decreased. For example, the membrane sample with stretching temperature increase from 35 °C (membrane sample 4) to 65 °C (membrane sample 8) leads to a decrease in membrane protein binding ability, which dropped from 4281 $\mu g/cm^3$ to 3446 $\mu g/cm^3$. This is due to the fact that, at high stretching temperature, membrane tends to have closed pore structure by the agglomeration of polymer matrix, as described previously. This closed pore structure is the main factor that contributes to protein binding resistance on the membrane's surfaces.

On the other hand, protein binding ability for a stretched membrane with higher stretching rate was higher compared to membrane with lower stretching rate, as shown in Figure 6c.
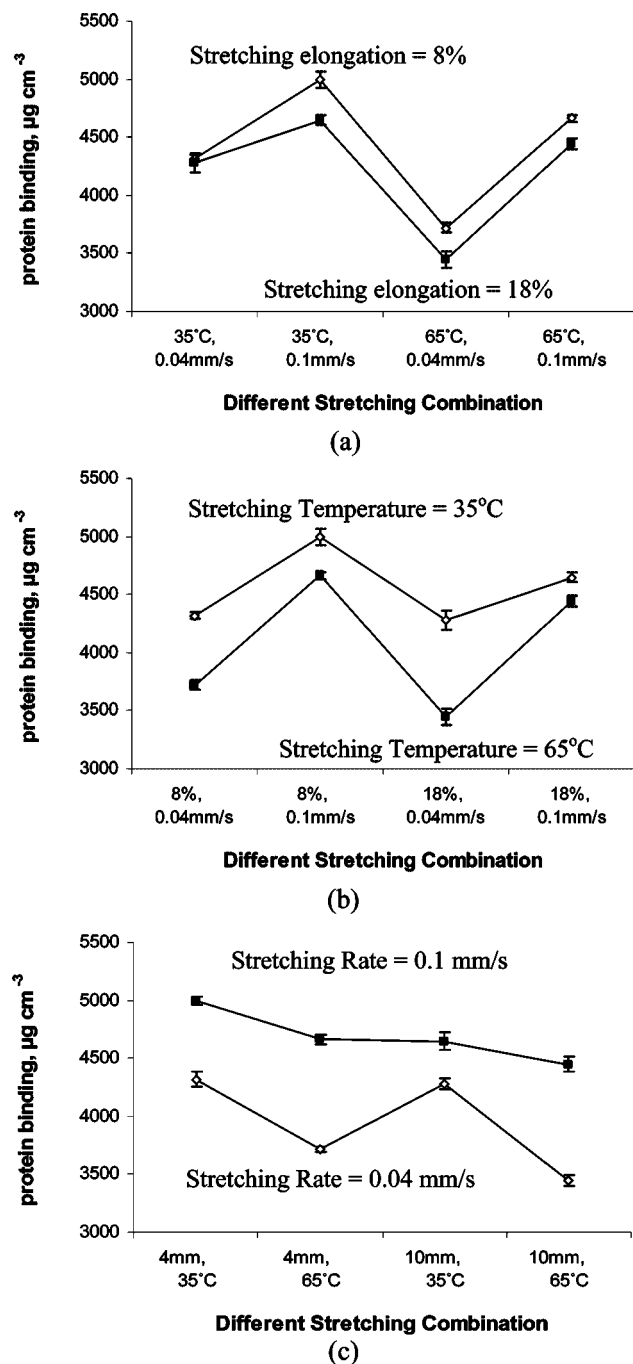
Figure 6. Effects of (a) stretching elongation, (b) stretching temperature, and (c) stretching rate on membrane protein binding ability. Each value represents an average value of three data points, and the bars represent the standard error.

The protein binding ability increased from 3716 μg/cm^3 to 4663 μg/cm^3 when the membrane stretching speed was increased from 0.04 mm/s to 0.1 mm/s. This is in line with the previous observation in membrane lateral migration speed, where higher stretching rate causes uneven force distribution on the membrane strip. The total surface area of membrane pores was higher, and more protein is able to bind onto membrane surfaces.

On the basis of the results from both Figures 5 and 6, it is clear that various stretching parameters on synthesized membrane would result in different membrane performances. Membrane protein binding ability decreased within 5% when the membrane stretching elongation was modified from 8% to 18% (Figure 6a). These changes were of less concern compared to the drastic increase of lateral wicking speed for the membrane.

Stretching elongation from 8% to 18% was able to speed up membrane wicking performance up to 25% (Figure 5a).

When the stretching temperature was increased from 35 to 65 °C, both protein binding ability and wicking speed were reduced. Membrane protein binding ability dropped up to 20% (Figure 6b), and membrane lateral wicking took up to 30% longer for liquid to migrate 4 cm in the lateral flow membrane (Figure 5b). This means that although the membrane could be easily stretched to longer elongation when the stretching temperature is high, the agglomeration of the polymer matrix pores would further reduce both the lateral flow and binding performances. However, the polymeric flat sheet membrane still needs to be stretched under the appropriate level of stretching temperature so that the polymer is ductile enough to be significantly stretched.

The membrane stretching rate has an opposite effects on the final membrane performances compared to the effects of membrane elongation. Higher stretching rate contributes to higher membrane binding ability (up to 29% in Figure 6c), but longer wicking time is needed (took up to 30% longer time) for the wicking medium to migrate across the membrane strip (Figure 5c). Hence, it is suggested that a moderate stretching rate, 0.07 mm/s, should be applied on future membrane stretching operation to maintain high membrane protein binding in the production of the diagnostic kit with rapid detection.

4. Conclusions

In summary, modification of membrane morphology through proposed uniaxial stretching operation is viable in improving the membrane performances. AFM and FESEM images clearly showed that the membrane surface morphologies are influenced by thermal-mechanical stretching operation. The experimental results indicated that pore structure and porosity of the membrane samples were dramatically changed due to the stretching effects. For membrane performance in lateral flow, increase of membrane stretching elongation would hasten the lateral wicking time but at the expense of lower protein binding ability on the membrane surface. Stretching elongation from 8% to 18% of the total membrane sample's length was able to increase the membrane wicking performance up to 25%, but there was only a 5% decrement on membrane protein binding. However, membrane produced using higher stretching temperature contributed to lower membrane protein binding ability, and longer time is needed for migration up to 4 cm height in the membrane strip. Although the membrane could be easily stretched when the stretching temperature was higher, the agglomeration of the polymer matrix pores would further reduce the membrane lateral performances. A moderate rate is recommended when stretching a membrane that can result in protein binding improvement and, at the same time, reduce the lateral migration time for rapid detection. These findings shed some light on the relationship between stretching setting and the stretched membrane performances. The ability of controlling membrane morphology through stretching operation could allow the membrane to be tailored for the production of versatile stretched membranes with specific uses and application. In this study, membrane morphology with optimum lateral flow performance was obtained by a membrane stretched to maximum elongation, moderate stretching rate, and minimum heating temperature during the stretching operation.

Literature Cited

(1) Lonnberg, M.; Carlsson, J. Chromatographic performance of a thin microporous bed of nitrocellulose. *J. Chromatogr. B* **2001**, *763* (1−2), 107–120.

(2) Qian, S.; Bau, H. H. Analysis of lateral flow biodetectors: competitive format. *Anal. Biochem.* **2004**, *326* (2), 211–224.

(3) Wang, J.; Johannsmann, D.; Hollas, M.; Thom, V. Visualization of capture line protein binding in nitrocellulose diagnostic membranes. *Desalination* **2006**, *199* (1−3), 232–233.

(4) Kesting, R. E. *Synthetic Polymer Membranes: A structural Perspective*, 2nd ed.; John Wiley & Sons Inc.: New York, 1985; pp 44−247.

(5) Pinnau, I.; Koros, W. J. A Qualitative Skin Layer Formation Mechanism for Membranes Made by Dry/Wet Phase Inversion. *J. Polym. Sci., Part B* **1993**, *31*, 419–417.

(6) Mulder, M. Chapter VI: Membrane Processes. In *Basic Principles of Membrane Technology*; 2nd ed.; Kluwer Academic Publishers: Dordrecht, The Netherlands, 2003; pp 280−393.

(7) Kurumada, K.-i.; Kitamura, T.; Fukumoto, N.; Oshima, M.; Tanigaki, M.; Kanazawa, S.-i. Structure generation in PTFE porous membranes induced by the uniaxial and biaxial stretching operations. *J. Membr. Sci.* **1998**, *149* (1), 51–57.

(8) Huang, J.; Zhang, J.; Hao, X.; Guo, Y. Study of a new novel process for preparing and co-stretching PTFE membrane and its properties. *Eur. Polym. J.* **2004**, *40* (4), 667–671.

(9) Green, D. L.; McAmish, L.; McCormick, A. V. Three-dimensional pore connectivity in bi-axially stretched microporous composite membranes. *J. Membr. Sci.* **2006**, *279* (1−2), 100–110.

(10) Li, C.; Liu, J.; Guan, R.; Zhang, P.; Zhang, Q. Effect of heating and stretching membrane on ionic conductivity of sulfonated poly(phenylene oxide). *J. Membr. Sci.* **2007**, *287* (2), 180–186.

(11) Morehouse, J. A.; Worrel, L. S.; Taylor, D. L.; Lloyd, D. R.; Freeman, B. D.; Lawler, D. F. The effect of uni-axial orientation on macroporous membrane structure. *J. Porous Mater.* **2006**, *13* (1), 61–72.

(12) Morehouse, J. A.; Taylor, D. L.; Lloyd, D. R.; Lawler, D. F.; Freeman, B. D.; Worrel, L. S. The effect of uni-axial stretching on the roughness of microfiltration membranes. *J. Membr. Sci.* **2006**, *280* (1−2), 712–719.

(13) Lee, N.; Amy, G.; Croue, J.-P.; Buisson, H. Morphological analyses of natural organic matter (NOM) fouling of low-pressure membranes (MF/UF). *J. Membr. Sci.* **2005**, *261* (1−2), 7–16.

(14) Dietz, P.; Hansma, P. K.; Inacker, O.; Lehmann, H.-D.; Herrmann, K.-H. Surface pore structures of micro- and ultrafiltration membranes imaged with the atomic force microscope. *J. Membr. Sci.* **1992**, *65* (1−2), 101–111.

(15) Richard Bowen, W.; Doneva, T. A. Atomic force microscopy studies of nanofiltration membranes: surface morphology, pore size distribution and adhesion. *Desalination* **2000**, *129* (2), 163–172.

(16) Ahmad, A. L.; Low, S. C.; Shukor, S. R. A. Effects of membrane cast thickness on controlling the macrovoid structure in lateral flow nitrocellulose membrane and determination of its characteristics. *Scr. Mater.* **2007**, *57* (8), 743–746.

(17) Ahmad, A. L.; Low, S. C.; Shukor, S. R. A.; Asma, I. Synthesis and characterization of polymeric nitrocellulose membranes: Influence of additives and pore formers on the membrane morphology. *J. Appl. Polym. Sci.* **2008**, *108* (4), 2550–2557.

(18) Binke, N.; Rong, L.; Xianqi, C.; Yuan, W.; Rongzu, H.; Qingsen, Y. Study on the melting process of nitrocellulose by thermal analysis method. *J. Therm. Anal. Calorim.* **1999**, *58* (2), 249–256.

(19) Yamane, S.; Takayama, K.; Nagai, T. Effect of fractal dimension on drug permeation through porous ethylcellulose films. *J. Controlled Release* **1998**, *50* (1−3), 103–109.

(20) Meier, M. M.; Kanis, L. A.; Soldi, V. Characterization and drug-permeation profiles of microporous and dense cellulose acetate membranes: influence of plasticizer and pore forming agent. *Int. J. Pharm.* **2004**, *278* (1), 99–110.

(21) Pristoupil, T. I.; Kramlova, M.; Sterbikova, J. On the mechanism of adsorption of proteins to nitrocellulose in membrane chromatography. *J. Chromatogr. A* **1969**, *42*, 367–375.

(22) Van Oss, C. J.; Good, R. J.; Chaudhury, M. K. Mechanism of DNA (southern) and protein (western) blotting on cellulose nitrate and other membranes. *J. Chromatogr. A* **1987**, *391*, 53–65.

(23) Al-Jeshi, S.; Neville, A. An investigation into the relationship between flux and roughness on RO membranes using scanning probe microscopy. *Desalination* **2006**, *189* (1−3), 221–228.